A Stylized Computational Model of the Rat for Organ Dosimetry in Support of Preclinical Evaluations of Peptide Receptor Radionuclide Therapy with ^{90}Y, ^{111}In, or ^{177}Lu

Mark W. Konijnenberg, PhD[1]; Magda Bijster[2]; Eric P. Krenning, MD, PhD[2]; and Marion de Jong, PhD[2]

[1]Mallinckrodt Medical, Tyco Healthcare, Petten, The Netherlands; and [2]Department of Nuclear Medicine, Erasmus Medical Center Rotterdam, Rotterdam, The Netherlands

The therapeutic effects of peptide receptor–based radionuclide therapy are extensively being investigated in rats bearing tumors. Both the dose to the tumor and the therapy-limiting dose to normal tissues, such as kidneys and bone marrow, are of interest for these preclinical studies. The aim of this work was to develop a generalized computational model for internal dosimetry in rats. **Methods:** Mature rats were dissected and the relative positions, dimensions, and weights of all of their major organs were measured. A mathematic model was set up for the rat body and its internal organs to enable Monte Carlo radiation transport calculations to determine estimates for both tumor and organ self-doses as cross-organ doses for ^{90}Y, ^{111}In, and ^{177}Lu. The organs and body were mostly of ellipsoid shape with the axes given as the measured length, width, and height normalized to values that, together with the measured weights, are consistent with the recommended soft-tissue and bone densities. A spheric tumor of 0.25 g was positioned on the right femur. Calculations were performed with the Monte Carlo neutral particle transport code MCNP for the β-emitters (maximum energy, 2.28 MeV) and ^{177}Lu (maximum energy, 0.497 MeV) and for the γ-emissions from ^{177}Lu and from ^{111}In. The presented absorbed dose S values are used to calculate the absorbed dose estimates for the rat organs in a study on the biodistribution of ^{177}Lu-DOTA-Tyr^3-octreotate (DOTA is 1,4,7,10-tetraazadodecane-*N,N′,N″,N‴*-tetraacetic acid). Three activity distributions were considered in the kidney: uniform in the whole kidney, in the cortex, or in the outer 1-mm-thick rim of the cortex. Isodose curves and dose volume histograms were calculated for the dose distribution to the kidneys. **Results:** Depending on the activity distribution in the kidneys, the renal dose for ^{177}Lu-DOTA-Tyr^3-octreotate is 0.13–0.17 mGy/MBq. **Conclusion:** The renal dose of 70–95 Gy for an injected activity of 555 MBq will likely cause radiation damage, although the higher amount of peptide with this activity may influence the dosimetry by partial receptor saturation. Dose volume histograms show that ^{111}In and ^{177}Lu are likely to have a higher threshold for renal damage than ^{90}Y.

Received Nov. 3, 2003; revision accepted Jan. 29, 2004.

For correspondence or reprints contact: Mark W. Konijnenberg, PhD, Mallinckrodt Medical BV, P.O. Box 3, 1755 ZG Petten, The Netherlands.

E-mail: mark.konijnenberg@emea.tycohealthcare.com

Key Words: autoradiography; radiobiology or dosimetry; radionuclide therapy; ^{111}In; ^{177}Lu; S factors; ^{90}Y; rat dosimetry model

J Nucl Med 2004; 45:1260–1269

Scintigraphy with ^{111}In-DTPA-octreotide (DTPA is diethylenetriaminepentaacetic acid) (Octreoscan; Mallinckrodt Medical, Inc.) has proven itself to be a very sensitive and specific method to localize somatostatin receptor–positive tumors and their metastases. Continuing research is aimed at developing a therapeutic analog, taking advantage of the specificity of the receptor binding and the localized radiation dose from the radionuclide linked to the peptide. As ^{111}In emits 2 γ-rays, it is not optimal for therapy usage. Instead, ^{90}Y-DOTA-Tyr^3-octreotide (DOTA is 1,4,7,10-tetraazadodecane-*N,N′,N″,N‴*-tetraacetic acid), with the high-energy β-emitter ^{90}Y (mean energy, 0.93 MeV; half-life [$t_{1/2}$], 64 h) strongly linked in the DOTA-cage, has been developed and is now clinically being evaluated (*1–3*) for an optimized peptide receptor radionuclide therapy (PRRT). ^{90}Y-DOTA-Tyr^3-octreotide lacks γ-emission itself or a γ-ray–emitting diagnostic analog. Discrepancies between the renal uptakes of the positron-emitting analog ^{86}Y-DOTA-Tyr^3-octreotide and of ^{111}In-DTPA-octreotide obscure the possibility of using the latter for dosimetry (R. Barone, written communication, November 2003 (*4*)). ^{177}Lu ($t_{1/2}$, 6.7 d) emits β-particles (mean energy, 0.13 MeV) as well as γ-rays suitable for imaging (113 keV at 6% per decay and 208 keV at 10% per decay). Together with a slightly altered somatostatin analog—octreotate, in which the amino acid threoninol at the C-terminal side of the octopeptide has been replaced by threonine—^{177}Lu-DOTA-Tyr^3-octreotate forms a superior therapeutic compound with considerably enhanced uptake in receptor-positive tumors (*5,6*).

The therapeutic effects of peptide receptor–based radionuclide therapy are extensively being investigated in studies with rats bearing tumors (*7–10*). It has been possible to

observe tumor regression and, consequently, survival in a study of the effects of ^{177}Lu-DOTA-Tyr^3-octreotate in a rat model (*7,9*). Not only is the dose to the tumor of interest for these preclinical studies, but also is the therapy-limiting dose to normal tissues, such as kidneys and bone marrow. Using human dosimetry S values to estimate the dosimetry in the rat organs, as performed in the study by Lewis et al. (*7*), to explain observed toxicity introduces difficulties by the large difference in the dimensions from rat to human, as will be shown in this article.

Internal dosimetry for radionuclides depends on the dose estimation model used; in humans, the MIRD schema provides a generalized anatomic model with which the doses to all internal organs can be calculated from the organ residence times for the considered radionuclide (*11*). However, for the dosimetry of radionuclides applied in animals, no general models exist apart from the mouse model of Hui et al. (*12*), in which only ^{90}Y dosimetry was considered. With the emphasis on the bone marrow dose for high-energy β-emitters, the authors concluded that low-energy β-emitters would also benefit from cross-organ radiation transport calculations. Dose volume histograms (DVHs) and 3-dimensional (3D) dosimetry for mouse liver, spleen, and kidney were introduced by Kolbert et al. (*13*). Suborgan dosimetry for mouse kidneys with differentiation of the cortex and medulla has been performed by Flynn et al. (*14*). These authors showed that the activity and dose distribution in the cortex is highly dependant on both the size of the antibody to which the activity is bound and to the range of the β-rays. The dose in the cortex can be >3 times larger than the dose in the medulla, and also within the cortex the dose may vary over 50%. A recently presented model by Hindorf et al. (*15*) for both mice and rats in a voxel-based geometry showed the relative insensitivity to organ shape (elliptic vs. spheric) and emphasized the importance of good interorgan positioning for dosimetry.

The aim of this work was to develop a generalized stylized calculational model for internal dosimetry of rats. Mature rats were dissected and the relative positions, dimensions, and weights of all of their major organs were measured. A mathematic model was set up for the rat body and its internal organs to enable Monte Carlo radiation transport calculations to determine estimates for both tumor and organ self-doses as cross-organ doses for ^{90}Y, ^{111}In, and ^{177}Lu. The presented absorbed dose S values are used to calculate the absorbed doses for the rat organs in a study on the biodistribution of ^{177}Lu-DOTA-Tyr^3-octreotate (*9*).

MATERIALS AND METHODS

Three mature well-fed Wistar rats (average weight, 386 ± 35 g) were dissected and the dimensions and weights of the liver, spleen, kidneys, lungs, heart, stomach, small and large bowel, thyroid, femur and its bone marrow, testes, bladder, and carcass (Table 1) were measured. The relative positions of these organs within the rat body were based on the photograph of a dissected rat (Fig. 1) as well as on the topologic capability of fitting all organs within the rat outer body contour. The organs and body were modeled as ellipsoids with their axes given as the length, width, and height of each organ as measured within the dissected animals (Figs. 2 and 3). The skull, brain, spine, and spinal core dimensions were not actually measured but were estimated to a shape fitting inside the outer body contour. The dimensions were normalized to the measured organ weights to make them consistent with the recommended ICRU Report 46 soft-tissue and bone densities (*16*). To have a maximum cross-dose to the marrow cavity, a small spheric tumor of 0.25 g was positioned within the right femur. The defining mathematic equations and parameters used for the organs and body contour are listed in the Appendix.

TABLE 1
Average Organ Dimensions of 3 Wistar Rats Weighing 386 ± 35 g

Organ	Length (cm)	Width (cm)	Height (cm)	Mass (g)
Liver	4.7	3.6	2.3	21.9
Spleen	3.1	0.5	0.6	0.8
Kidney				
Whole	2.2	1.4	1	1.7
Renal surface*	*2.0*	*1.2*	*0.8*	*1.06*
Renal cortex*	*1.45*	*0.9*	*0.6*	*1.26*
Lungs	3.2	2.7	0.8	1.6
Heart	1.9	1.3	1.1	1.8
Stomach	3.3	2.1	1.4	6.2
Small bowel	3	2.3	0.6	10
Large bowel	4	4.1	1.1	14.5
Thyroid	0.9	0.4	0.1	0.06
Pancreas	2.8	1.1	0.4	1.4
Femur	3.6	0.4	0.1	1.2
Marrow	2.3	0.2	0.2	0.05
Bladder	1	0.7	0.3	0.1
Testis	2	2	1	1.8
Skull*	*1.7*	*3.2*	*4*	*8.3*
Brain*	*1.5*	*3*	*3*	*7.3*
Spine*	*18*	*0.4*	*0.5*	*4.3*
Spinal core*	*18*	*0.2*	*0.2*	*0.58*
Total body	25.8	7.3	3.3	312.1

*Values in italic type are estimated dimensions; all other values were actually measured.

Calculations were performed with MCNP4C (*17*) for the β-emitters ^{90}Y (maximum energy, 2.28 MeV) and ^{177}Lu (maximum energy, 0.498 MeV) and for the Auger electron and γ-emissions from ^{111}In and ^{177}Lu. Specific β-spectra were obtained from the ICRP 38 database (*18*), the particle energy and emission probabilities for ^{177}Lu were from Schötzig et al. (*19*), and the Auger electron spectrum for ^{111}In was from Howell (*20*). The lower cutoff value for the energy for photons and β-rays was set at 0.01 MeV; for the low-energy Auger and internal conversion electrons, the threshold was set at 0.001 MeV. The number of electron histories needed to obtain acceptable absorbed energy fractions (ϕ) (statistical error < 5%) in adjacent organs is 500,000 for the β-rays from ^{90}Y and ^{177}Lu. The γ- and low-energy electron part of the ^{111}In and ^{177}Lu emission needed 1,000,000 histories. All source activities were distributed homogeneously over the source organs. The dosimetry to the femur bone was performed following Eckerman and Stabin (*21*). All bone marrow in the rat's femur,

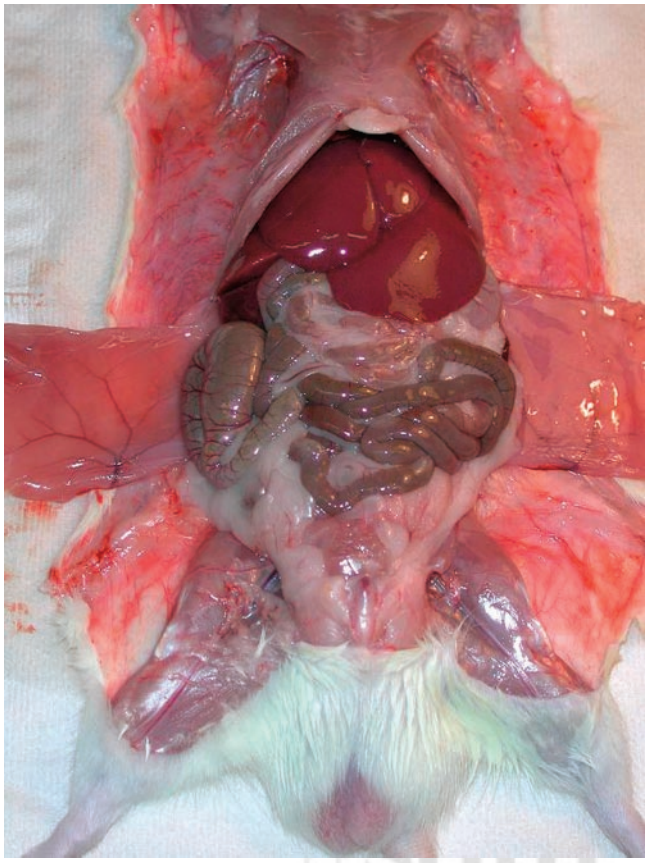

FIGURE 1. Cut-open view of one of analyzed rats shows lungs, liver, pancreas, and bowel.

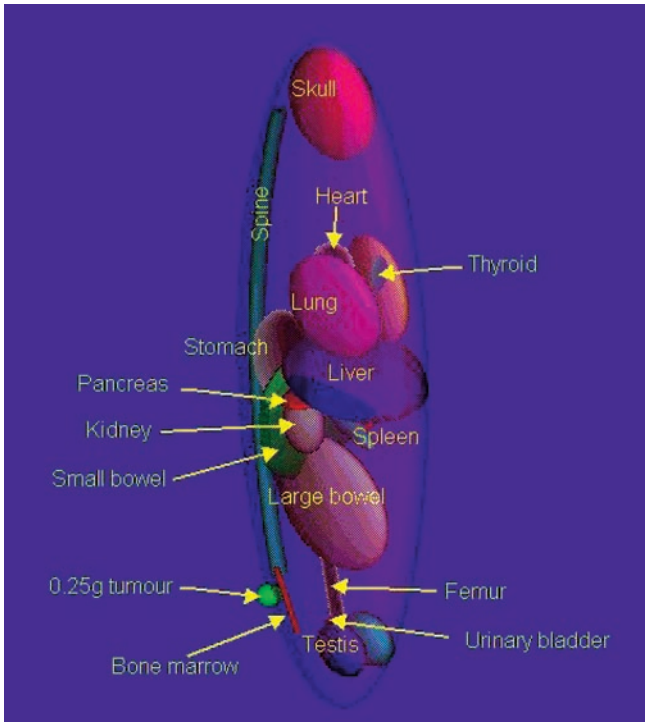

FIGURE 2. Visualization of stylized model of rat in MCNP4C with small tumor on hind leg.

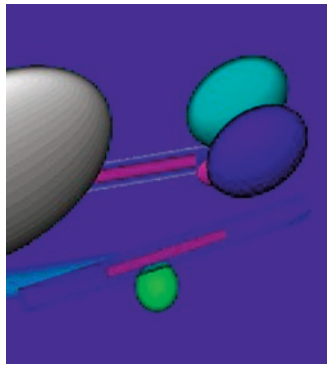

FIGURE 3. Expanded view of tumor (green) on semitransparent femur shown with its marrow contents. All non-organ soft tissues and skin have been omitted.

however, is known to be active (red) marrow, unlike the human situation (*21*).

For the kidney uptake, selective uptake in the cortex and in an outer 1-mm-thick layer of the cortex was considered also. Autoradiography of the kidneys of rats injected with ^{177}Lu-DOTA-octreotate showed selective uptake in the outer part of the cortex (*9*,*22*). The dimensions of the kidneys were therefore measured from these autoradiographs as well as the size of the cortex and the surface layer with the highest radioactivity uptake. In the kidneys, 3 distributions were analyzed: (a) homogeneous in the whole kidney; (b) homogeneous in the renal cortex; and (c) in the outside surface layer of the cortex, as shown in Figure 4. Four suborgan target regions were taken in the kidney: the renal cortex, the renal surface layer, the pelvis, and the whole kidney. As rat kidneys have a single lobe, the pelvis also includes the medulla. The dose distribution over the kidney was analyzed by separate Monte Carlo calculations for each activity distribution, using a 1-mm voxel-scoring grid over all kidney regions. By taking 10^6 electron and 2×10^6 photon histories, a compromise was made between the obtained accuracy in each voxel (~8%) and the total calculation time (~12 and 28 h on a Pentium III [Intel Corp.] personal computer, respectively). The dose distributions are visualized by isodose contours as well as by DVHs.

RESULTS

Absorbed fractions of energy emitted for the 0.25-g tumor model on one of the hind legs of the rat with incorporated ^{90}Y, ^{111}In, and ^{177}Lu are given in Table 2. The Auger electrons of ^{111}In and ^{177}Lu are essentially all absorbed

FIGURE 4. Cross-section through central planes of kidney model with 1-mm-thick surface (dark brown), rest of cortex (light brown), and pelvis region (gray). Adjacent organs are pancreas (light purple), liver (dark purple), small bowel (yellow), and spleen (light gray).

TABLE 2
Absorbed Fractions of Emitted Energy (ϕ) in Rat Femur Tumor Model for ^{90}Y, ^{111}In, and ^{177}Lu

Source		Target (%)		
		Tumor	Femur	Marrow
Tumor	^{90}Y	51	3.7	0.5
	^{111}In (γ-rays)	0.9	0.3	0.0
	^{111}In (Au/IC e$^-$)	96	0.2	0.0
	^{177}Lu (β-rays)	94	0.3	0.0
	^{177}Lu (γ-rays)	0.9	0.4	0.0
	^{177}Lu (Au/IC e$^-$)	98	0.1	0.0
Femur	^{90}Y	4.6	36	7.5
	^{111}In (γ-rays)	0.1	1.0	0.1
	^{111}In (Au/IC e$^-$)	2.0	53	11
	^{177}Lu (β-rays)	2.1	51	11
	^{177}Lu (γ-rays)	0.1	1.2	0.1
	^{177}Lu (Au/IC e$^-$)	1.7	57	10
Marrow	^{90}Y	1.7	43	27
	^{111}In (γ-rays)	0.1	1.1	0.4
	^{111}In (Au/IC e$^-$)	0.0	9.0	91
	^{177}Lu (β-rays)	0.0	12	87
	^{177}Lu (γ-rays)	0.1	1.2	0.4
	^{177}Lu (Au/IC e$^-$)	0.0	3.3	97

Auger (Au) and internal conversion (IC) electron part of ^{111}In and ^{177}Lu emissions was considered (for ^{111}In: 14.8 Au/IC e$^-$/decay with E_{mean} = 2.3 keV; for ^{177}Lu: 0.25 Au/IC e$^-$/decay with E_{mean} = 30 keV).

within the source organ itself. Only for the femur as a source organ does the self-dose for Auger electrons differ considerably from unity.

For most organs, the β-part of the emissions from ^{177}Lu is completely absorbed within the organ itself ($\phi \geq 95\%$). The higher-energy β-rays from ^{90}Y show a higher probability for escape from source organs and, therefore, will produce higher cross-organ doses. For instance, the energy absorption in the femur's bone surface from activity in the tumor is 3.7% for ^{90}Y and well below 1% for the other nuclides. The absorbed dose S values are calculated by converting MeV per decay to mGy·g/MBq·s and dividing by the target organ mass. The complete tables with S values are given in the Appendix. For the results of radioactivity uptake experiments with younger and smaller rats, the absorbed dose can be corrected by dividing by the organ mass ratio of these rats compared with the masses given in Table 1. Here, it is additionally assumed that corresponding changes in ϕ are not appreciable.

Kidney Model

Special attention was given to the effect of several activity distributions in the kidney; the results are given in Tables 3 and 4. For ^{90}Y, the absorbed fraction in the whole kidney reduces from 71% to 55% when the activity distribution is changed from whole kidney to a surface source. The absorbed energy fraction in the cortex, however, barely shows a change between the 2 distributions: 48% versus 49%. With ^{177}Lu, there is a 29% increase in the total S value to the

TABLE 3
Absorbed Fractions ϕ in Rat Kidney Model

Source		Target (%)			
		Kidneys	Cortex	Surface	Pelvis
Kidneys	^{90}Y	70.9	48.4	20.8	22.5
	^{111}In (γ-rays)	1.6	1.1	0.5	0.5
	^{111}In (Au/IC e$^-$)	97.9	72.6	35.8	25.3
	^{177}Lu (β-rays)	96.8	71.4	34.6	25.4
	^{177}Lu (γ-rays)	1.7	1.2	0.5	0.5
	^{177}Lu (Au/IC e$^-$)	99.2	73.7	36.9	25.5
Cortex	^{90}Y	64.9	54.0	24.7	11.0
	^{111}In (γ-rays)	1.5	1.1	0.6	0.3
	^{111}In (Au/IC e$^-$)	97.3	96.2	47.8	1.1
	^{177}Lu (β-rays)	95.8	94.2	46.3	1.7
	^{177}Lu (γ-rays)	1.6	1.2	0.6	0.3
	^{177}Lu (Au/IC e$^-$)	98.9	98.5	49.3	0.4
1-mm surface	^{90}Y	55.2	48.9	31.3	6.3
	^{111}In (γ-rays)	1.3	1.1	0.6	0.3
	^{111}In (Au/IC e$^-$)	94.8	94.7	90.9	0.001
	^{177}Lu (β-rays)	91.8	91.8	85.9	0.001
	^{177}Lu (γ-rays)	1.4	1.1	0.7	0.3
	^{177}Lu (Au/IC e$^-$)	97.8	97.8	96.2	0.001

Au = Auger electron; IC = internal conversion electron.
Radioactivity is either distributed homogeneously over kidney or cortex or in 1-mm outer surface layer of cortex.

TABLE 4
Radiation Dose Estimates per Cumulated Activity S (Target ← Source) in mGy/MBq · s for ^{90}Y and Different Radiation Components of ^{177}Lu in Several Source Distributions Within Rat Kidney

Source		Target			
		Kidneys	Cortex	Surface	Pelvis
Kidneys	^{90}Y	3.14E−02	2.87E−02	2.45E−02	3.92E−02
	^{111}In (γ-rays)	3.17E−04	2.94E−04	2.64E−04	3.84E−04
	^{111}In (Au/IC e$^-$)	1.56E−03	1.55E−03	1.51E−03	1.58E−03
	^{111}In (total)	1.88E−03	1.84E−03	1.78E−03	1.97E−03
	^{177}Lu (β-rays)	6.10E−03	6.03E−03	5.79E−03	6.30E−03
	^{177}Lu (γ-rays)	4.38E−06	2.33E−05	2.11E−05	3.05E−05
	^{177}Lu (Au/IC e$^-$)	6.85E−04	6.82E−04	6.76E−04	6.91E−04
	^{177}Lu (total)	6.79E−03	6.74E−03	6.49E−03	7.02E−03
Cortex	^{90}Y	2.88E−02	3.21E−02	2.91E−02	1.91E−02
	^{111}In (γ-rays)	2.93E−04	3.06E−04	2.84E−04	2.57E−04
	^{111}In (Au/IC e$^-$)	1.55E−03	2.06E−03	2.02E−03	6.81E−05
	^{111}In (total)	1.85E−03	2.36E−03	2.31E−03	3.25E−04
	^{177}Lu (β-rays)	6.05E−03	7.97E−03	7.76E−03	4.13E−04
	^{177}Lu (γ-rays)	2.20E−05	2.30E−05	2.27E−05	2.05E−05
	^{177}Lu (Au/IC e$^-$)	6.84E−04	9.13E−04	9.06E−04	1.21E−05
	^{177}Lu (total)	6.75E−03	8.91E−03	8.69E−03	4.46E−04
1-mm surface	^{90}Y	2.44E−02	2.91E−02	3.68E−02	1.09E−02
	^{111}In (γ-rays)	2.63E−04	2.84E−04	3.25E−04	2.00E−04
	^{111}In (Au/IC e$^-$)	1.51E−03	2.02E−03	3.84E−03	6.01E−08
	^{111}In (total)	1.77E−03	2.31E−03	4.17E−03	2.00E−04
	^{177}Lu (β-rays)	5.79E−03	7.77E−03	1.44E−02	3.83E−07
	^{177}Lu (γ-rays)	2.09E−05	2.26E−05	2.58E−05	1.59E−05
	^{177}Lu (Au/IC e$^-$)	6.74E−04	9.04E−04	1.76E−03	2.85E−08
	^{177}Lu (total)	6.49E−03	8.69E−03	1.62E−02	1.63E−05

Au = Auger electron; IC = internal conversion electron.

cortex when the activity is distributed over the surface instead of the whole kidney, mainly due to the β-rays in the ^{177}Lu emissions. For ^{111}In, this increase is comparable: 25% and, despite the short range of its electrons, 5% of the emitted energy does not get absorbed in the cortex with a surface source distribution. The isodose curves for ^{90}Y, ^{177}Lu, and ^{111}In in Figure 5 show these findings graphically. For ^{90}Y, the inner boundary of the cortex aligns with the 80% isodose curve for the cortex activity distribution and with the 50% isodose curve for the surface activity distribution. In the case of ^{111}In and ^{177}Lu, this boundary corresponds with the 60% isodose curve for the cortex and with the 10% isodose curve for the surface distribution.

The volume distribution of the dose is best visible with the DVHs, as shown in Figure 6. A uniform dose will show an almost rectangular shape as seen with ^{111}In and ^{177}Lu for the whole kidney and cortex activity distributions. There is a slight falloff of the dose at the boundaries, but the dose in the renal cortex is, for these cases, well described by the average dose. For ^{90}Y, the falloff is slightly larger, but already 16% of the cortex volume receives a dose below 0.024 mGy/MBq·s, or 25% below the average value in the case of the cortex distribution. When the activity is distributed in the outer 1-mm surface layer of the cortex, all nuclides show an irregular DVH. Not surprisingly, doses for ^{90}Y appear to be less affected by the source distribution. ^{177}Lu gets a very low dose ($<6 \times 10^{-4}$ mGy/MBq·s, or 7% of the average) in 25% of the cortex volume. With ^{111}In, there is a lower threshold value by the longer-ranged γ-radiation, but still 25% of the cortex volume gets a dose below 3×10^{-4} mGy/MBq·s, or 13% of the average. For comparison with ^{90}Y, the dose sparing at the inner cortex boundary yields a mere 4% of the cortex volume with a dose below 0.015 mGy/MBq·s, or 52% of the average. On the maximum side, ^{90}Y also does not produce extremely higher doses for the surface distribution (10% cortex volume $>$ 0.036 mGy/MBq·s, or 1.23 $\times$ average). For ^{111}In and ^{177}Lu, these values are much more extreme (for ^{111}In: 10% $>$ 0.0039 mGy/MBq·s, or 1.68 $\times$ average; for ^{177}Lu: 10% $>$ 0.015 mGy/MBq·s, or 1.75 $\times$ average).

Uptake of ^{177}Lu-DOTA-Tyr^3-Octreotate in Rats

The biodistribution of ^{177}Lu-DOTA-Tyr^3-octreotate was determined in tumor-bearing rats at several time intervals (*9*). ^{177}Lu-DOTA-Tyr^3-octreotate was intravenously injected at a specific activity of 3 MBq ^{177}Lu per 0.5 μg peptide. The results are presented in Table 5. An exponential curve was fitted to the data, using the numeric option in the SAAM II code (SAAM Institute). The blood clearance showed a rapid clearance phase (99.9% with 24-min $t_{1/2}$)

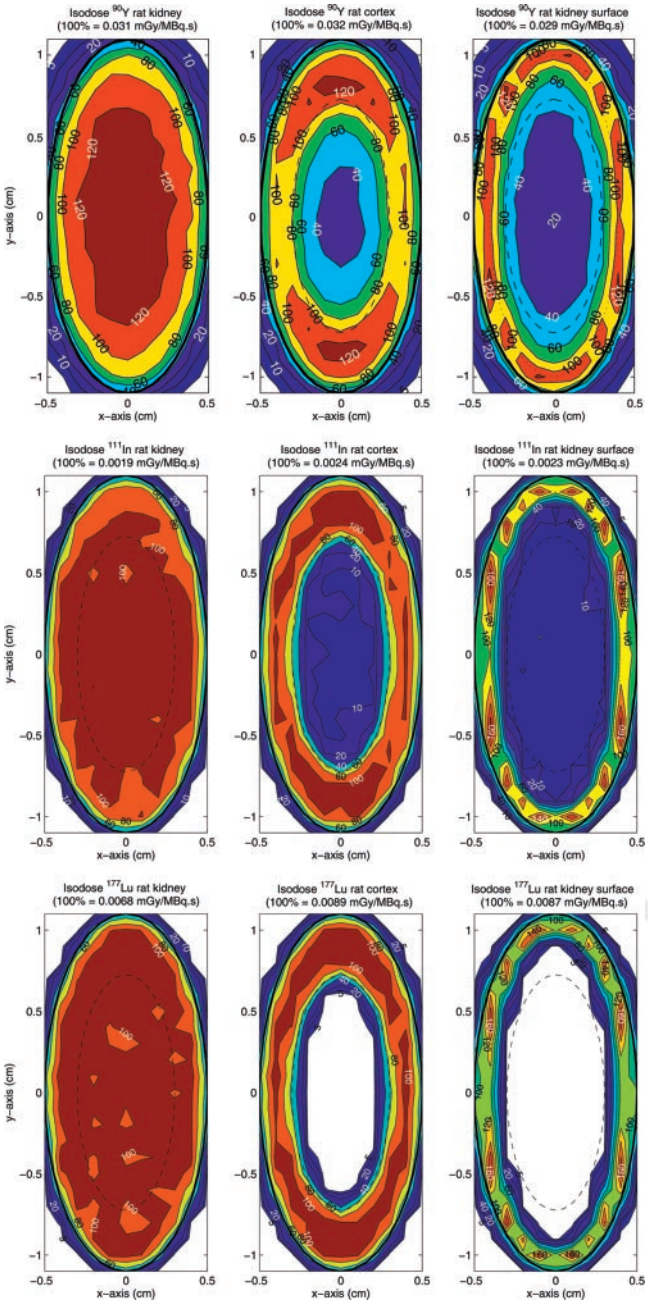

FIGURE 5. Isodose curves for ^{90}Y, ^{111}In, and ^{177}Lu in longitudinal plane of kidneys for activity distributions: 1, kidneys; 2, renal cortex; 3, cortex surface layer of 1-mm thickness. The 5%, 10%, 20%, 40%, 60%, 80%, 100%, 120%, 140%, and 160% of average isodose curves are indicated.

and a very small redistribution phase (0.07% with 17-h $t_{1/2}$ and 0.02% with infinite $t_{1/2}$). The same fitting procedure was performed on the uptake data by Lewis et al. (*7*) and the results are shown in Table 5 for comparison.

With escalation of the injected activities to levels higher than considered in this dosimetry study, the increased mass of peptide administered (assuming constant specific activity) will cause lower uptake in receptor-positive organs. Partial saturation of the receptors is causing this effect, which has been shown to potentially lower the uptake in the tumor with 50% (*9*,*23*). The dosimetry values for the receptor-positive organs in rats (adrenals, pancreas, pituitary, and stomach) and tumors are only valid at the peptide mass used in this study.

The injected activities to the rats were escalated to 555 MBq, leading to a kidney dose of 72 and 49 Gy, respectively, for both datasets. If the activity is taken up in the cortex, the dose to the cortex goes up to 95 and 64 Gy, respectively. For an activity uptake just in the outer 1-mm surface layer of the cortex, the dose in this surface layer is 172 Gy and the mean dose to the cortex becomes 92 Gy (115 and 63 Gy (*7*)). It can be derived from the DVHs that for a surface distribution the dose in the cortex varies between 5 Gy (12% volume) and 165 Gy (5% volume). The other distributions show a D_{05} (5% of the volume is exceeding this dose) comparable to the mean cortex dose: D_{05}(cortex) = 104 Gy and D_{05}(kidney) = 79 Gy. In external-beam radiotherapy, the effective volume method is used to characterize nonuniformly irradiated normal organs (*24*,*25*); this method yields the following effective volumes: V_{eff}(kidney) = 74%, V_{eff}(cortex) = 72%, and V_{eff}(surface) = 40%.

DISCUSSION

Normal tissue radiation toxicity in rats from radiolabeled compounds can now be compared on a dose level (in Gy) instead of injected activities (in MBq). The advantage of such an approach is apparent; it clears the uncertainty in upscaling from injected activities in rats to the equivalent in humans (*26*). However, the influence of high mass amounts of peptides on the biodistribution, when administering activities at normal organ radiation toxicity levels in rat experiments, limits the use of the dose values for receptor-positive organs determined at lower peptide concentrations (*23*). Fortunately, the uptake in the kidneys is not receptor mediated. Both the effects as well as the use of human dosimetry in the evaluation of dose effects in rats by ^{177}Lu-DOTA-Tyr^3-octreotate obscure the conclusions of the otherwise excellent work by Lewis et al. (*7*). For instance, their kidney dose estimate of 0.670 ± 0.047 mGy/MBq does not indicate any probability of finding radiation damage in the kidneys with an injected activity of 555 MBq, leading to a minimal renal dose of 0.37 Gy. Using the rat-based dosimetry of this article, the dose of 49 Gy for a uniform distribution over the kidneys is more in the range where renal damage for fractionated radiation can be expected (*27*). The doses in the range of 63–64 Gy by a more localized activity distribution will likely cause observable effects in the kidneys.

Evaluation of the effects by a nonuniform radiation distribution in the kidneys by PRRT cannot be directly inferred

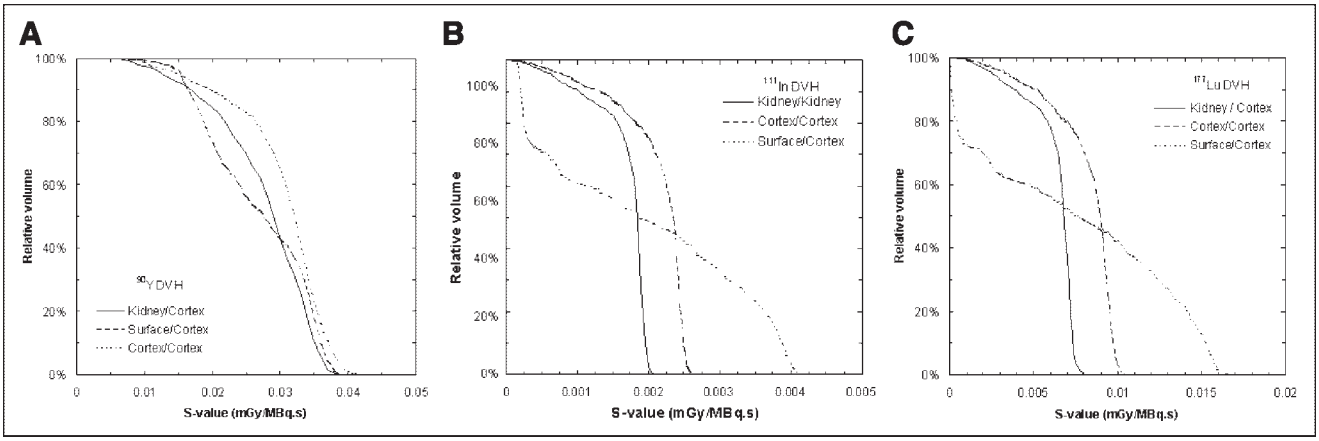

FIGURE 6. DVHs for absorded dose to renal cortex for ^{90}Y (A), ^{111}In (B), and ^{177}Lu (C) activity distributions as described in Figure 4.

from the extensive experience in radiobiology with external beams. With PRRT the distribution is related to physiologic uptake in the kidneys, whereas for x-ray irradiation anatomic contours and external-beam modifiers define the distribution. The effective volume method assumes that the functional units are uniformly distributed over the considered volume. It is still uncertain for rat kidneys whether the glomeruli, which form the radiation-sensitive functional units for late damage, are evenly distributed over the cortex, whereas in human kidneys the majority of the glomeruli are placed in the outer cortical regions (*28*).

Behr and Béhé (*29*) observed a remarkable difference in toxicity in preclinical therapy experiments with DTPA-D-Glu^1-minigastrin labeled with either ^{90}Y or ^{111}In in tumor-bearing mice. ^{90}Y induced chronic nephropathy at a renal dose of ≥60 Gy, whereas renal damage for ^{111}In was found at approximately twice this dose. Dosimetry for ^{90}Y may be influenced by the large difference in volume of a mouse kidney (0.15–0.18 cm^3 (*13*)) and a rat kidney (1.6 cm^3), by both differences in ϕ (52% vs. 71%) as well as differences in the radiation distributions. The much lower range of the ^{111}In Auger electrons, however, will yield quite comparable radiation distribution patterns in mouse and rat kidneys. The findings by Behr and Béhé can be explained by the DVHs. For an average kidney dose of 60 Gy the DVHs, with ^{90}Y and ^{111}In distributed in the outer cortex surface, are shown in Figure 7. With ^{111}In 45% of the cortical volume gets a dose of <10 Gy, whereas for ^{90}Y the cortex dose exceeds 20 Gy almost (99%) everywhere. It is currently not known whether minigastrin shows the same uptake pattern in the kidneys as found for octreotate.

TABLE 5
Organ Masses, Residence Times (τ), and Dose per Injected Activity for ^{177}Lu-DOTA-Tyr^3-Octreotate in Rats According to Uptake Data of de Jong et al. and Lewis et al.

	de Jong et al. (*9*)			Lewis et al. (*7*)		
Organ	Mass (g)	τ (min)	Dose (mGy/MBq)	Mass (g)	τ (min)	Dose (mGy/MBq)
Blood	13	14		18	11	
Pancreas	0.93	186	260*	1.2	194	216*
Adrenals	0.05	26		0.04	16	
Kidneys	2.1	200	130	2.2	133	89
Liver	10	40	5.8	11	26	3.6
Stomach	1.6	57	50*	4.6	40	12*
Thymus	0.46	3.3	8.8	0.44	2.5	6.9
Pituitary	0.02	3.0		0.009	3.4	
Femur	1	2.3	6.7	1	49	48
Muscle	118	13	0.39	37	9.2	0.72
Spleen	0.66	2.5	5.6	0.55	1.5	4.1
CA20948†	3	476	212*	1.2	205	225*

*For pancreas, adrenals, stomach, pituitary, and tumor, uptakes and dose per injected activity are only valid at used peptide mass of 0.5 μg with 3 MBq ^{177}Lu (*9*) or 0.67 μg with 1.3 MBq ^{177}Lu (*7*).

†CA20948 tumors.

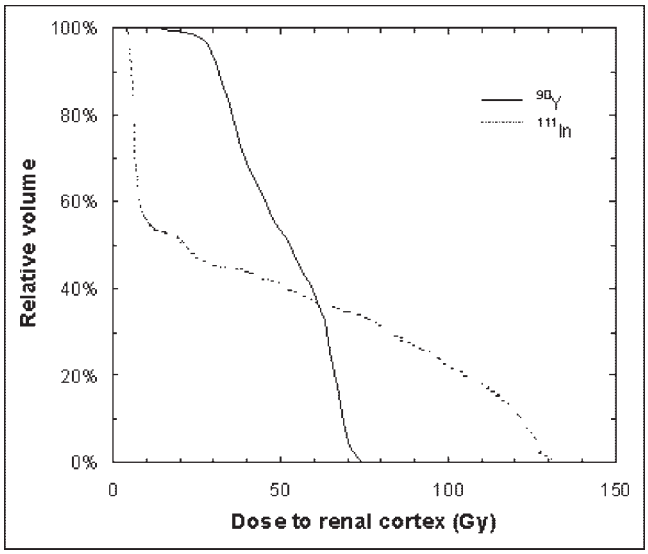

FIGURE 7. DVH for renal cortex dose by activities of ^{90}Y and ^{111}In that produce average dose to kidneys of 60 Gy, when uniformly distributed in kidneys. Activity distribution is over renal cortex surface.

CONCLUSION

A general-purpose stylized model rat is presented, for which the S factors for ^{90}Y, ^{111}In, and ^{177}Lu have been calculated. Dosimetry was performed for a biodistribution experiment with ^{177}Lu-DOTA-octreotate. DVHs and isodose lines were calculated for 3 types of radioactivity distributions within the kidneys, showing a large deviation from a uniform distribution to a more realistic distribution in the supracortical region of the kidneys. With the distribution pattern for octreotate renal uptake, DVHs show that ^{111}In and ^{177}Lu are likely to have a higher threshold for renal damage than ^{90}Y, like the experience with minigastrin (*29*).

APPENDIX

The defining mathematic equations and parameters used for the organs and body contour are given in Table A1. The absorbed dose S values for ^{111}In, ^{177}Lu, and ^{90}Y are given in Tables A2, A3, and A4, respectively.

TABLE A1
Mathematic Definitions and Parameters Used for Stylized Rat Model

Ellipsoids	$\left(\frac{x-x_0}{a}\right)^2+\left(\frac{y-y_0}{b}\right)^2+\left(\frac{z-z_0}{c}\right)^2=1$						Angle with *z*-axis
Organ	*a* (cm)	*b* (cm)	*c* (cm)	x_0 (cm)	y_0 (cm)	z_0 (cm)	θ
Liver	1.8	2.35	1.15	0	1	0.5	0°
Spleen	0.3	1.6	0.375	0.5	1.25	−1	−13°
Kidney	0.5	0.7	1.1	±1	0	−1.5	0°
Surface	0.4	0.6	1.0	±1	0	−1.5	0°
Cortex	0.3	0.45	0.725	±1	0	−1.5	0°
Lungs	0.475	1.6	1.9	±0.75	1	3.5	±10°
Heart	0.6	0.7	1.0	0	0	4	0°
Stomach	0.75	1.1	1.75	0	−2	−0.5	0°
Small bowel	1.9	0.5	2.5	0	−1	−2	0°
Large bowel	0.63	2.31	2.36	0	0	−5	0°
Thyroid	0.29	0.074	0.66	0	2	5	0°
Pancreas	1.8	0.5	0.26	0	0	−0.5	0°
Bladder wall	0.2	0.5	0.625	0	−0.25	−10	0°
Contents	0.15	0.45	0.575	0	−0.25	−10	0°
Testis	0.47	0.94	0.94	±0.47	1.0	−10	0°
Skull	0.85	1.6	4.0	0	0	10.5	0°
Brain	0.75	1.5	1.5	0	0	10.5	0°
Body contour	1.65	13.3	12.9	0	0	0	0°

Cylinders	$(x-x_0)^2+(y-y_0)^2=r^2$ with $\lvert z-z_0\rvert \le A$					Angle
Organ	*r* (cm)	*A* (cm)	x_0 (cm)	y_0 (cm)	z_0 (cm)	θ
Femur	0.2	5.55	±0.79	−1	−9	±4.5°
Marrow	0.1	2.3	±0.79	−1	−9	±4.5°

Elliptical tori	$\left(\frac{x}{b}\right)^2+\left(\frac{\sqrt{(y-\bar{y})^2+z^2}-a}{c}\right)^2=1$, with $\lvert z\rvert \le 9$ and $y<0$			
	a (cm)	*b* (cm)	*c* (cm)	$\bar{y}$ (cm)
Spine	42.5	0.25	0.2	39.25
Spinal core	42.5	0.1	0.1	39.25

TABLE A2
Absorbed Dose S Values (in mGy/MBq · s) for ^{111}In

Sources→ ↓Targets	Liver	Spleen	Kidneys	Lungs	Heart	Stomach	S. bowel	L. bowel	Thyroid	Tumor	Pancreas	Bone	Marrow	Ur. bl. co.	Testis	Carcass
Liver	9.49E−03	4.18E−05	2.32E−05	1.60E−05	1.14E−05	1.78E−05	1.42E−05	3.61E−06	5.70E−06	6.69E−07	6.16E−05	5.45E−08	7.27E−07	3.95E−08	5.77E−07	8.76E−06
Spleen	8.65E−05	4.94E−01	1.76E−04	1.40E−05	9.68E−06	2.87E−05	4.43E−05	1.62E−05	5.78E−06	2.13E−06	2.05E−04	9.86E−08	2.40E−06	1.14E−07	1.98E−06	2.59E−05
Kidneys	7.27E−05	1.93E−04	1.88E−03	1.44E−05	1.31E−05	7.56E−05	1.71E−04	3.71E−05	6.92E−06	4.25E−06	3.16E−04	1.24E−07	4.52E−06	2.45E−07	3.55E−06	3.36E−05
Lungs	1.25E−04	5.07E−05	3.48E−05	4.70E−01	5.89E−04	3.95E−05	2.72E−05	9.80E−06	4.13E−04	2.32E−06	6.22E−05	2.56E−08	2.61E−06	1.61E−07	2.00E−06	8.95E−05
Heart	4.87E−05	2.22E−05	1.93E−05	3.53E−04	5.51E−01	2.57E−05	1.57E−05	5.34E−06	1.36E−04	1.34E−06	3.09E−05	2.46E−08	1.54E−06	6.86E−08	1.42E−06	6.86E−05
Stomach	6.59E−05	5.22E−05	8.78E−05	1.92E−05	2.20E−05	1.14E−01	1.62E−04	2.03E−05	7.84E−06	3.69E−06	1.20E−04	8.92E−08	3.88E−06	1.98E−07	2.76E−06	3.66E−05
S. bowel	8.14E−05	1.25E−04	3.24E−04	2.00E−05	1.92E−05	2.52E−04	1.27E−01	1.26E−04	9.32E−06	1.14E−05	2.51E−04	1.58E−07	1.23E−05	6.36E−07	7.32E−06	5.84E−05
L. bowel	2.46E−05	5.27E−05	7.88E−05	8.65E−06	7.36E−06	3.73E−05	1.48E−04	9.26E−02	4.47E−06	4.67E−05	4.30E−05	7.07E−07	5.78E−05	3.05E−06	3.34E−05	8.19E−05
Thyroid	1.62E−04	7.53E−05	4.83E−05	1.45E−03	6.10E−04	5.71E−05	3.94E−05	1.25E−05	1.91E+00	2.74E−06	8.63E−05	1.05E−08	4.94E−06	2.54E−09	1.31E−05	4.36E−04
Tumor	7.79E−07	9.77E−07	1.17E−06	2.08E−07	2.83E−07	1.32E−06	1.77E−06	7.29E−06	1.39E−07	2.11E−02	1.03E−06	4.18E−04	2.98E−04	4.24E−06	1.97E−05	8.35E−06
Pancreas	3.44E−04	5.58E−04	6.15E−04	4.59E−05	3.96E−05	1.87E−04	2.52E−04	3.66E−05	1.77E−05	5.47E−06	2.41E−02	7.77E−08	5.82E−06	3.28E−07	3.11E−06	5.72E−05
Bone surf.	9.48E−07	2.14E−06	1.52E−07	8.03E−07	2.56E−07	2.08E−06	5.47E−06	1.75E−05	3.26E−07	1.90E−04	2.22E−06	3.76E−03	9.23E−04	1.81E−06	4.23E−05	6.53E−04
Bone vol.	1.84E−06	3.00E−06	4.57E−06	8.30E−07	8.22E−07	3.01E−06	6.39E−06	2.57E−05	4.80E−07	1.78E−04	2.79E−06	1.72E−03	8.95E−04	4.96E−05	5.83E−05	2.29E−05
Marrow	7.07E−07	1.25E−06	1.28E−06	3.76E−07	2.35E−07	1.02E−06	2.36E−06	9.38E−06	2.71E−07	1.69E−04	1.16E−06	3.61E−03	3.18E−02	8.63E−06	2.66E−05	1.13E−05
Bladder	4.30E−06	3.73E−06	8.92E−06	2.26E−06	2.18E−06	4.58E−06	1.17E−05	3.69E−05	1.21E−06	2.66E−04	3.74E−06	6.31E−06	5.47E−04	3.04E−01	6.10E−04	9.20E−05
Testes	4.94E−06	9.03E−06	9.91E−06	2.52E−06	2.11E−06	6.59E−06	1.26E−05	4.75E−05	1.47E−06	1.45E−04	7.22E−06	2.08E−06	2.42E−04	1.29E−04	1.51E−02	7.52E−05
Carcass	7.89E−06	1.08E−05	9.75E−06	1.03E−05	1.15E−05	8.78E−06	9.08E−06	1.08E−05	1.45E−05	7.39E−06	8.94E−06	6.74E−06	9.32E−06	1.43E−06	7.23E−06	2.89E−05
Sp. chord	3.97E−06	3.37E−06	4.38E−06	3.46E−06	5.63E−06	2.27E−05	8.15E−06	6.59E−06	2.18E−06	7.98E−06	5.47E−06	5.09E−07	6.46E−06	2.21E−07	1.78E−06	9.93E−06

S. bowel = small bowel; L. bowel = large bowel; Ur. bl. co. = urinary bladder contents; bone surf. = bone surface; bone vol. = bone volume; Sp. chord = spinal chord.

TABLE A3
Absorbed Dose S Values (in mGy/MBq · s) for ^{177}Lu

Sources→ ↓Targets	Liver	Spleen	Kidneys	Lungs	Heart	Stomach	S. bowel	L. bowel	Thyroid	Tumor	Pancreas	Bone	Marrow	Ur. bl. co.	Testis	Carcass
Liver	1.09E−03	3.60E−06	1.87E−06	1.29E−06	8.95E−07	2.23E−06	1.82E−06	2.80E−07	4.45E−07	5.14E−08	2.03E−05	5.48E−08	5.44E−08	4.39E−08	4.32E−08	1.49E−06
Spleen	3.73E−06	2.82E−02	1.44E−05	5.58E−07	3.96E−07	1.18E−06	1.83E−06	6.44E−07	2.28E−07	8.86E−08	2.49E−05	9.86E−08	9.85E−08	7.21E−08	6.85E−08	5.06E−06
Kidneys	1.81E−06	4.84E−06	6.79E−03	3.60E−07	3.29E−07	1.86E−06	9.94E−06	9.03E−07	1.79E−07	9.96E−08	5.81E−05	1.18E−07	1.16E−07	8.21E−08	7.97E−08	3.02E−06
Lungs	1.39E−06	5.47E−07	2.77E−06	7.51E−03	4.66E−05	4.07E−07	2.85E−07	1.01E−07	4.45E−06	2.34E−08	6.60E−07	2.54E−08	2.72E−08	2.45E−08	1.95E−08	9.50E−06
Heart	7.81E−07	3.66E−07	1.52E−06	3.82E−05	1.29E−02	4.15E−07	2.55E−07	8.43E−08	2.18E−06	2.06E−08	5.01E−07	2.47E−08	2.17E−08	1.76E−08	1.71E−08	3.24E−06
Stomach	2.35E−06	1.15E−06	7.16E−06	4.14E−07	4.85E−07	3.66E−03	1.18E−05	4.42E−07	1.70E−07	7.75E−08	2.66E−06	8.99E−08	8.46E−08	6.22E−08	5.40E−08	2.14E−06
S. bowel	1.64E−06	1.55E−06	6.20E−05	2.43E−07	2.33E−07	9.90E−06	2.26E−03	4.44E−06	1.12E−07	1.35E−07	7.48E−06	1.57E−07	1.56E−07	1.06E−07	8.96E−08	1.96E−06
L. bowel	2.82E−07	6.16E−07	6.29E−06	9.64E−08	8.45E−08	4.34E−07	5.05E−06	1.57E−03	4.97E−08	5.35E−07	5.00E−07	7.07E−07	6.71E−07	4.16E−07	3.89E−07	2.57E−06
Thyroid	4.90E−07	2.73E−07	3.24E−06	4.56E−06	1.80E−06	2.29E−07	1.36E−07	4.80E−08	3.28E−01	2.08E−08	2.52E−07	1.05E−08	2.63E−08	7.86E−09	1.99E−08	1.51E−05
Tumor	6.45E−08	7.66E−08	1.21E−07	2.60E−08	2.47E−08	9.66E−08	1.54E−07	5.77E−07	1.04E−08	8.90E−02	6.24E−08	2.01E−03	2.32E−05	3.06E−06	1.40E−06	3.34E−06
Pancreas	1.95E−05	2.30E−05	3.53E−04	5.50E−07	4.96E−07	2.31E−06	7.31E−06	4.72E−07	2.15E−07	6.76E−08	1.57E−02	7.68E−08	7.29E−08	5.14E−08	5.85E−08	2.60E−06
Bone surf.	3.88E−08	8.74E−08	6.24E−07	2.79E−08	1.61E−08	8.09E−08	1.11E−07	5.81E−07	5.35E−09	4.50E−05	6.30E−08	1.62E−02	1.44E−03	4.53E−06	1.55E−06	5.15E−06
Bone vol.	7.57E−08	1.31E−07	3.70E−07	3.38E−08	2.98E−08	1.34E−07	2.76E−07	1.16E−06	1.89E−08	3.61E−05	1.20E−07	4.16E−03	1.12E−03	7.52E−06	2.58E−06	4.08E−06
Marrow	5.13E−08	8.49E−08	8.18E−08	2.05E−08	1.67E−08	7.71E−08	1.98E−07	6.88E−07	1.70E−08	1.33E−05	9.82E−08	1.74E−02	1.39E−01	6.94E−06	2.17E−06	8.75E−07
Bladder	5.98E−08	5.71E−08	6.26E−07	2.29E−08	1.80E−08	8.19E−08	1.39E−07	4.46E−07	1.88E−08	3.22E−06	5.28E−08	6.29E−06	6.81E−06	1.68E−02	7.79E−06	1.56E−05
Testes	4.20E−08	7.24E−08	7.00E−07	1.98E−08	1.94E−08	5.46E−08	1.08E−07	4.16E−07	1.20E−08	1.26E−06	6.14E−08	2.08E−06	2.12E−06	7.75E−06	6.39E−03	3.01E−06
Carcass	1.61E−06	5.30E−06	2.66E−06	9.13E−06	3.02E−06	2.25E−06	2.33E−06	2.68E−06	1.49E−05	2.99E−06	3.06E−06	3.53E−05	8.63E−07	1.46E−06	3.01E−06	9.68E−05
Sp. chord	3.04E−07	2.64E−07	3.55E−07	2.80E−07	4.29E−07	1.75E−06	6.43E−07	5.14E−07	1.74E−07	6.16E−07	4.30E−07	5.08E−07	5.04E−07	2.57E−07	1.32E−07	8.00E−07

S. bowel = small bowel; L. bowel = large bowel; Ur. bl. co. = urinary bladder contents; bone surf. = bone surface; bone vol. = bone volume; Sp. chord = spinal chord.

TABLE A4
Absorbed Dose S Values (in mGy/MBq · s) for ^{90}Y

Sources→ ↓ Targets	Liver	Spleen	Kidneys	Lungs	Heart	Stomach	S. bowel	L. bowel	Thyroid	Tumor	Pancreas	Bone	Marrow	Ur. bl. co.	Testis	Carcass
Liver	5.92E−03	2.13E−04	2.54E−05	4.63E−05	2.37E−07	7.48E−05	5.02E−05	4.14E−08	9.06E−08	1.19E−08	1.03E−03	1.37E−08	9.57E−09	5.23E−09	2.61E−09	4.63E−05
Spleen	2.28E−04	1.06E−01	2.32E−03	8.04E−08	3.90E−08	4.44E−07	1.07E−05	8.55E−08	9.79E−09	5.12E−19	2.68E−03	7.37E−19	6.57E−09	3.20E−19	3.64E−19	2.09E−04
Kidneys	2.60E−05	5.68E−04	3.14E−02	7.97E−08	5.42E−08	6.44E−07	6.12E−04	3.10E−07	3.33E−08	2.84E−09	2.80E−03	1.99E−08	1.26E−08	4.55E−09	7.31E−09	1.18E−04
Lungs	4.49E−05	5.49E−08	4.27E−07	1.77E−02	3.00E−03	1.29E−07	7.05E−08	5.51E−09	1.49E−03	2.49E−19	1.08E−07	6.65E−10	2.88E−19	1.03E−09	1.65E−19	3.39E−04
Heart	1.23E−07	7.44E−08	2.18E−07	2.49E−03	6.03E−02	6.57E−08	1.82E−08	4.27E−09	3.23E−06	2.04E−09	1.45E−07	1.06E−08	1.03E−20	8.47E−10	3.99E−20	1.36E−04
Stomach	8.25E−05	3.12E−07	2.04E−06	1.02E−07	6.99E−08	1.93E−02	5.77E−04	7.88E−08	3.28E−08	2.29E−08	3.29E−05	4.69E−08	2.65E−08	8.78E−09	3.72E−09	8.83E−05
S. bowel	4.72E−05	1.14E−05	3.64E−03	2.75E−08	4.78E−08	4.92E−04	1.13E−02	1.91E−04	1.04E−08	5.41E−08	4.63E−04	3.17E−08	2.51E−08	8.77E−09	1.00E−08	7.45E−05
L. bowel	3.42E−08	1.12E−07	3.02E−06	1.23E−08	4.19E−09	8.90E−08	2.12E−04	8.33E−03	1.24E−08	7.40E−08	7.37E−08	2.34E−07	1.55E−07	7.54E−08	5.94E−08	1.07E−04
Thyroid	4.87E−09	3.20E−18	1.29E−17	1.55E−03	2.86E−06	6.83E−18	3.01E−18	7.54E−19	6.66E−01	1.26E−18	4.69E−18	8.48E−19	0.00E+00	0.00E+00	0.00E+00	4.02E−04
Tumor	9.24E−20	1.39E−19	4.51E−19	1.70E−07	0.00E+00	3.27E−08	1.32E−18	5.93E−09	0.00E+00	3.07E−01	4.90E−20	2.78E−02	1.04E−02	5.93E−07	1.38E−07	1.03E−04
Pancreas	9.82E−04	2.40E−03	1.66E−02	1.07E−07	1.27E−07	2.62E−05	4.73E−04	5.54E−08	1.19E−08	2.42E−10	5.98E−02	9.51E−09	6.74E−10	8.73E−09	2.71E−08	7.97E−05
Bone surf.	1.02E−17	1.60E−17	1.17E−32	1.06E−17	4.08E−18	7.25E−18	3.02E−17	2.25E−07	3.10E−18	5.30E−04	9.66E−18	8.88E−03	5.50E−03	6.85E−05	1.12E−06	3.42E−05
Bone vol.	2.30E−08	4.30E−08	8.85E−08	3.71E−19	2.97E−09	3.47E−09	1.10E−07	9.93E−07	6.99E−09	2.28E−03	3.41E−08	2.18E−02	2.65E−02	3.15E−04	5.41E−06	1.62E−04
Marrow	5.98E−19	1.10E−18	2.62E−18	1.33E−18	0.00E+00	0.00E+00	3.31E−18	1.06E−17	0.00E+00	5.15E−03	3.87E−19	7.55E−02	2.68E−01	9.03E−05	1.57E−06	1.57E−04
Bladder	4.98E−19	1.17E−07	3.10E−17	1.61E−19	0.00E+00	7.91E−19	1.90E−18	8.92E−18	0.00E+00	7.92E−07	1.82E−18	1.53E−04	2.20E−04	1.84E−01	1.58E−03	3.47E−04
Testes	1.50E−10	7.71E−09	6.69E−08	2.76E−09	1.07E−19	1.64E−08	3.38E−08	8.25E−08	1.91E−20	1.91E−07	2.66E−10	3.10E−06	8.69E−07	1.10E−03	3.04E−02	1.14E−04
Carcass	5.13E−05	2.21E−04	1.04E−04	3.44E−04	1.28E−04	8.95E−05	8.75E−05	1.10E−04	4.32E−04	1.12E−04	9.50E−05	2.74E−04	1.46E−04	2.67E−04	1.16E−04	5.21E−04
Sp. chord	2.64E−08	1.26E−07	2.79E−08	1.58E−08	1.10E−07	1.71E−04	6.13E−08	2.23E−07	3.78E−09	2.86E−07	4.24E−08	8.51E−08	1.43E−07	2.09E−09	2.46E−18	1.25E−04

S. bowel = small bowel; L. bowel = large bowel; Ur. bl. co. = urinary bladder contents; bone surf. = bone surface; bone vol. = bone volume; Sp. chord = spinal chord.

REFERENCES

1. Smith MC, Liu J, Chen T, et al. OctreoTher: ongoing early clinical development of a somatostatin-receptor-targeted radionuclide antineoplastic therapy. *Digestion.* 2000;62(suppl 1):69–72.
2. Bodei L, Cremonesi M, Zoboli S, et al. Receptor-mediated radionuclide therapy with ^{90}Y-DOTATOC in association with amino acid infusion: a phase I study. *Eur J Nucl Med Mol Imaging.* 2003;30:207–216.
3. Waldherr C, Pless M, Maecke HR, et al. Tumor response and clinical benefit in neuroendocrine tumors after 7.4 GBq ^{90}Y-DOTATOC. *J Nucl Med.* 2002;43:610–616.
4. Helisch A, Förster GJ, Reber H, et al. Pre-therapeutic dosimetry and biodistribution of ^{86}Y-DOTA-Phe^{1}-Tyr^{3}-octreotide versus ^{111}In-pentetreotide in patients with advanced neuroendocrine tumours. *Eur J Nucl Med Mol Imaging.* June 3, 2004 [Epub ahead of print].
5. de Jong M, Breeman WAP, Bakker WH, et al. Comparison of ^{111}In-labeled somatostatin analogues for tumor scintigraphy and radionuclide therapy. *Cancer Res.* 1998;58:437–441.
6. Kwekkeboom DJ, Bakker WH, Kam BL, et al. Treatment of patients with gastro-entero-pancreatic (GEP) tumours with the novel radiolabelled somatostatin analogue [^{177}Lu-DOTA^{0},Tyr^{3}]octreotate. *Eur J Nucl Med Mol Imaging.* 2003;30:417–422.
7. Lewis JS, Wang M, Laforest R, et al. Toxicity and dosimetry of ^{177}Lu-DOTA-Y^{3}-octreotate in a rat model. *Int J Cancer.* 2001;94:873–877.
8. Stolz B, Weckbecker G, Smith-Jones PM, et al. The somatostatin receptor-targeted radiotherapeutic [^{90}Y-DOTA-D-Phe^{1},Tyr^{3}]octreotide (^{90}Y SMT487) eradicates experimental rat pancreatic CA20948 tumours. *Eur J Nucl Med.* 1998;25:668–674.
9. de Jong M, Breeman WAP, Bernard BF, et al. [^{177}Lu-DOTA^{0},Tyr^{3}]octreotate for somatostatin receptor-targeted radionuclide therapy. *Int J Cancer.* 2001;92:628–633.
10. de Jong M, Breeman WAP, Bernard BF, et al. Tumor response after [^{90}Y-DOTA^{0},Tyr^{3}]octreotide radionuclide therapy in a transplantable rat tumor model is dependent on tumor size. *J Nucl Med.* 2001;42:1841–1846.
11. Stabin MG. MIRDOSE: personal computer software for internal dose assessment in nuclear medicine. *J Nucl Med.* 1996;37:538–546.
12. Hui TE, Fisher DR, Kuhn JA, et al. A mouse model for calculating cross-organ beta doses from yttrium-90-labeled immunoconjugates. *Cancer.* 1994;73(3 suppl):951–957.
13. Kolbert KS, Watson T, Matei C, et al. Murine S factors for liver, spleen, and kidney. *J Nucl Med.* 2003;44:784–791.
14. Flynn AA, Pedley RB, Green AJ, et al. The nonuniformity of antibody distribution in kidney and its influence on dosimetry. *Radiat Res.* 2003;159:182–189.
15. Hindorf C, Ljungbeg M, Strand SE. Dosimetric model for mice and rats [abstract]. *J Nucl Med.* 2003;44(suppl):150P.
16. ICRU report 46. *Photon, Electron, Proton and Neutron Interaction Data for Body Tissues.* Bethesda, MD: International Commission on Radiation Units and Measurements; 1992.
17. Briesmeister JF, ed. *MCNP: A General Monte Carlo N-Particle Transport Code.* Version 4C, LA-13709-M. Los Alamos, NM: Los Alamos National Laboratory; April 2000.
18. Eckerman KF, Westfall RJ, Ryman JC, Cristy M. Availability of nuclear data in electronic form, including beta spectra not previously published. *Health Phys.* 1994;67:338–345.
19. Schötzig U, Schrader H, Schonfeld E, et al. Standardisation and decay data of ^{177}Lu and ^{188}Re. *Appl Radiat Isot.* 2001;55:89–96.
20. Howell RW. Radiation spectra for Auger-electron emitting radionuclides: Report no. 2 of AAPM Nuclear Medicine Task Group no. 6. *Med Phys.* 1992;19:1371–1383.
21. Eckerman KF, Stabin MG. Electron absorbed fractions and dose conversion factors for marrow and bone by skeletal regions. *Health Phys.* 2000;78:199–214.
22. Breeman WAP, Van Der Wansem K, Bernard BF, et al. The addition of DTPA to [^{177}Lu-DOTA^{0},Tyr^{3}]octreotate prior to administration reduces rat skeleton uptake of radioactivity. *Eur J Nucl Med Mol Imaging.* 2003;30:312–315.
23. de Jong M, Breeman WAP, Bernard BF, et al. Tumour uptake of the radiolabelled somatostatin analogue [DOTA^{0},TYR^{3}]octreotide is dependent on the peptide amount. *Eur J Nucl Med.* 1999;26:693–698.
24. Kutcher GJ, Burman C. Calculation of complication probability factors for non-uniform normal tissue irradiation: the effective volume method. *Int J Radiat Oncol Biol Phys.* 1989;16:1623–1630.
25. Dawson LA, Normolle D, Balter JM, et al. Analysis of radiation-induced liver disease using the Lyman NTCP model. *Int J Radiat Oncol Biol Phys.* 2002;53:810–821.
26. Sparks RB, Aydogan B. Comparison of the effectiveness of some common animal data scaling techniques in estimating human radiation dose. In: Stelson AT, Stabin MG, Sparks RB, eds. *Proceedings of the 6th International Radiopharmaceutical Dosimetry Symposium.* ORISE 99-0164. Gatlinburg, TN: Oak Ridge National Laboratories; 1996.
27. van Rongen E, Kuijpers WC, Madhuizen HT. Fractionation effects and repair kinetics in rat kidney. *Int J Radiat Oncol Biol Phys.* 1990;18:1093–1106.
28. Newbold KM, Sandison A, Howie AJ. Comparison of size of juxtamedullary and outer cortical glomeruli in normal adult kidney. *Virchows Arch A Pathol Anat Histopathol.* 1992;420:127–129.
29. Behr TM, Béhé MP. Cholestykin-B/gastrin receptor-targeting peptides for staging and therapy of medullary thyroid cancer and other cholecystokin-B receptor-expressing malignancies. *Semin Nucl Med.* 2002;32:97–109.